Journal of Power Sources 277 (2015) 403–415

Contents lists available at ScienceDirect

Journal of Power Sources

journal homepage: www.elsevier.com/locate/jpowsour

Impedance model of lithium ion polymer battery considering temperature effects based on electrochemical principle: Part I for high frequency

Meng Xiao, Song-Yul Choe*

Mechanical Engineering, 1418 Wiggins Hall, Auburn Univ., AL 36849, USA

HIGHLIGHTS

- Modeled double layer behavior on electrode surface of Li-ion battery.
- Employed modified Gouy-Chapman-Stern method in the model.
- Improved ion transport equation in electrolyte bulk.
- Analyzed the performance of separated sub-models as well as integrated model.

ARTICLE INFO

Article history:
Received 15 May 2014
Received in revised form
11 October 2014
Accepted 13 October 2014
Available online 29 October 2014

Keywords:
EIS
Double layer
Transference number
Pouch type Li-polymer battery
Electrochemical model

ABSTRACT

Measurement of impedance is one of well-known methods to experimentally characterize electrochemical properties of Li-ion batteries. The measured impedance responses are generally fitted to an equivalent circuit model that is composed of linear and nonlinear electric components that mimic behaviors of different layers of a battery. However, the parameters do not provide quantitative statements on charge dynamics considering material properties. Therefore, electrochemical models are widely employed to study the charge dynamics, but have not included high frequency responses predominantly determined by double layers. Thus, we have developed models for the double layer and bulk that are integrated into the electrochemical model for a pouch type Li-ion battery. The integrated model is validated against the frequency response obtained from EIS equipment at different temperatures as well as the time response. The results show that the proposed model is capable of representing the responses at charging and discharging in time and frequency domain.

1. Introduction

1.1. EIS and electric equivalent circuit model

Electrochemical Impedance Spectroscopy (EIS) is the technique that has been widely used to study performance of batteries. In 1986, Laman used the EIS to study effects of the geometry of a cylindrical Li-ion battery on performances [1]. The measured impedance of the terminal of the battery is approximated with that of an electric circuit with parameters derived from electrochemical behaviors of the battery. The electric circuit model was constructed by connecting resistors with capacitors and shows different responses in magnitude and phase when AC current or voltage with different frequency is applied at the terminal. Analysis on Li-ion batteries using the EIS conducted by Munichandraiah in 1998 revealed existence of three semicircles in complex domain. The semicircle formed at the high frequency range is caused by film resistance and its capacitance, and the one at the middle frequency range is from charge-transfer resistance and double layer (DL) capacitance, while the one at the low frequency range is due to diffusional impedance [2]. Effects of degradation on battery performance have not considered. Capacity fade of 18650 Li-ion cells at different operating conditions was investigated by Ning using the EIS, where an equivalent electric model was used and the parameters were extracted from the impedance data [3,4]. Analysis of the

* Corresponding author.
E-mail addresses: mzx0001@auburn.edu (M. Xiao), choe@auburn.edu (S.-Y. Choe).

http://dx.doi.org/10.1016/j.jpowsour.2014.10.157
0378-7753/

Nomenclature

A	Helmholtz free energy (J cm^{-3})
a	specific surface area for electrode (cm^{-1})
b	ion mobility (cm^2 V^{-1} s^{-1})
c	concentration (mol cm^{-3})
D	diffusion coefficient (cm^2 s^{-1})
F	Faraday's constant (96,487C mol^{-1})
e	energy storage density (J cm^{-1})
i_0	reference exchange current density (A cm^{-2})
I	load current (A)
j	transfer current density(A cm^{-3})
SOC	state of charge
N	ion flux (mol s^{-1} cm^{-2})
R	universal gas constant (8.3143 J mol^{-1} K^{-1})
T	cell temperature (K)
U	standard potential affected by solid concentration (V)
x	stoichiometric number in negative electrode or coordinate
y	stoichiometric number in positive electrode or coordinate

Greek symbols

ε	porosity of a porous medium
E	permittivity (F cm^{-1})
ϕ	potential in a phase (V)
η	surface overpotential (V)
σ	conductivity of solid active material (S cm^{-1})
μ	chemical potential (J mol^{-1})

Subscripts

a	anode reaction
B	bulk
c	cathode reaction
D	double layer
e	electrolyte phase
E	boundary between DL and bulk
eff.	effective
s	solid phase
S	boundary between DL and electrode particle
ST	stern plane
+	cathode
−	anode

parameters showed that the radius of the semicircle formed at low frequency range gets larger when cycled because of the increased interfacial resistance of both electrodes [5]. Another study using symmetric coin cells showed that the increased charge-transfer resistance is the main reason for degradation, where the charge-transfer resistance in cathode is larger than that in anode [6,7]. There has been another attempt to characterize interfacial behaviors for use of different solvents and salts along with different concentrations using the EIS [8]. Better correlation between the impedance and the parameters of the electric model was accomplished by replacing capacitors with constant phase elements (CPE) that are made of combined resistors and capacitors [9]. Other authors applied Kalman filter to correct the errors of the model [10,11].

All of the studies using EIS are based on the equivalent circuit model, which has several drawbacks. The electric equivalent circuit model (EECM) are constructed using lumped parameters that do not consider any effects of SOC or aging phenomena as well as locations, so that internal detailed mechanism associated with charge dynamics is hard to understand. The impedance is generally measured at an operating point with a perturbation of a small AC signal. When the operating point is changed, the impedance varies because of nonlinear behavior of the battery. Therefore, physical battery states cannot be accurately estimated by the linear parameters of electric equivalent circuit EIS model.

1.2. Current electrochemical model

Electrochemical model proposed by Doyle [12] has widely accepted to analyze static and dynamic behavior of ions in time domain. In frequency domain, however, the model does not show responses of impedance in high frequency range. The equations used for the model are summarized in table as below. These partial differential equations (PDEs) are discretized in two coordinates; spherical one for the radial direction (R direction) of particles and Cartesian one for through-the-plane direction (L direction) of the cell. The resulting matrices are solved with an implicit method. Details can be found in previously published papers [13,14].

Reaction kinetics

$$j^{\mathrm{Li}} = a_S \cdot i_0 \left(\exp\left(\frac{\alpha_a \cdot n \cdot F}{R \cdot T} \left(\eta - \eta_{\mathrm{SEI}} \right) \right) - \exp\left(-\frac{\alpha_c \cdot n \cdot F}{R \cdot T} \left(\eta - \eta_{\mathrm{SEI}} \right) \right) \right) \tag{1}$$

Electrolyte conductive

$$\frac{\partial}{\partial l}\left(\kappa_e^{\mathrm{eff}} \cdot \frac{\partial}{\partial l} \phi_e \right) + \frac{\partial}{\partial l}\left(\kappa_{D,e}^{\mathrm{eff}} \cdot \frac{\partial}{\partial l}\left(\ln c_e \right) \right) + j^{\mathrm{Li}} = 0 \tag{2}$$

Solid conductive

$$\frac{\partial}{\partial l}\left(\sigma^{\mathrm{eff}} \cdot \frac{\partial}{\partial l} \phi_s \right) = j^{\mathrm{Li}} \tag{3}$$

Electrolyte ion transport

$$\frac{\partial (\varepsilon_e c_e)}{\partial t} = \frac{\partial}{\partial l}\left(D_e^{\mathrm{eff}} \cdot \frac{\partial}{\partial l} c_e \right) + \frac{1 - t_+^0}{F} j^{\mathrm{Li}} \tag{4}$$

Solid ion transport

$$\frac{\partial c_s}{\partial t} = \frac{D_s}{r^2} \frac{\partial}{\partial r}\left(r^2 \frac{\partial c_s}{\partial r} \right) \tag{5}$$

In order to obtain frequency responses, AC signals with different frequencies are applied to the model and a pouch type lithium polymer battery using EIS equipment. The amplitude is 1 A and frequency ranges from 0.01 Hz to 900 Hz at 50% SOC. The results of the frequency responses are plotted in Fig. 1, where the real and imaginary parts of the calculated impedances in the low frequency range match fairly well with that of experiments, but not in the frequency that is larger than 20 Hz. The model does not respond on the high frequency excitations and remains constant even though the frequency increases. This discrepancy is more obvious at Nyquist plot that the simulation result with the current model shows a linearly increasing part, but completely misses the semicircle that represents high frequency responses.

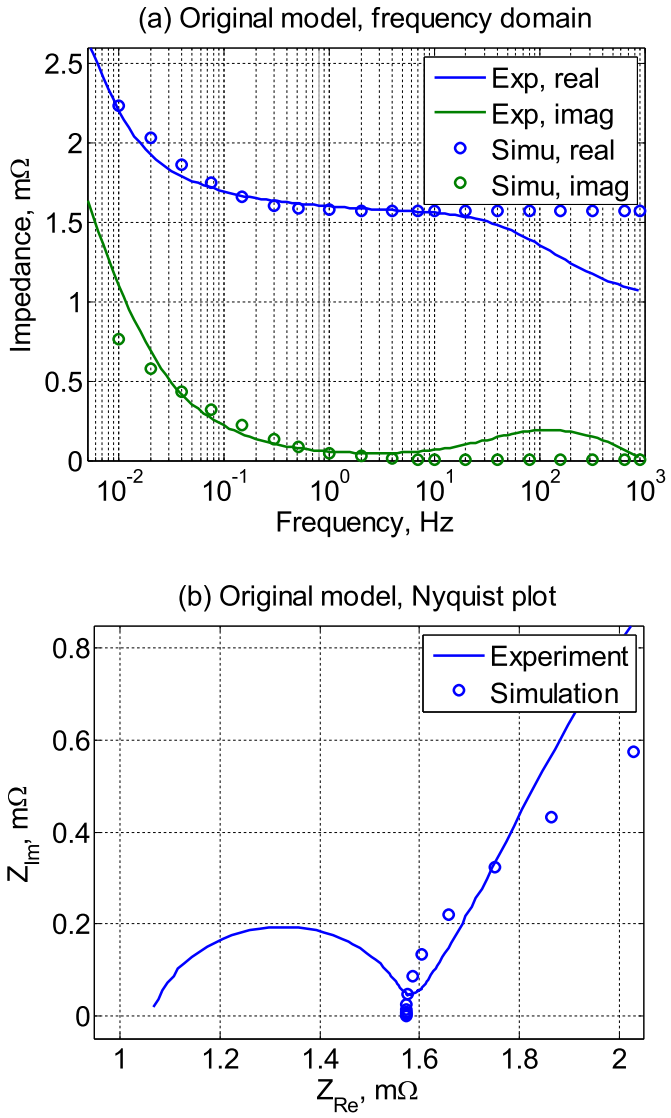

Fig. 1. Frequency response of original electrochemical model.

1.3. Review of models of double layer (DL)

The absence of the semicircle in the frequency response is caused by the neglected effects of the DL. There have been several attempts in the past. In 1999, Ong proposed a model for DL that basically consists of a resistor and a capacitor and included modified Butler–Volmer equation. The resulting electrochemical model was validated at discharging battery with a constant current [15]. Doyle derived an empirical equation for DL that considers dependence of overpotential on charges in DL, and incorporated into Butler–Volmer equation. The resulting model is transformed to a frequency domain model that is only a function of frequency [16].

Two approaches above used the electrochemical model to represent the frequency behavior of the Li-ion batteries, but are lacking clear correlations between the lumped parameters and physical operating conditions and material properties. In addition, the simulation results do not match experimental data well when the exciting signals are offset with DC components.

The DL responsible for the high frequency part of EIS was firstly observed in the charged mercury drop experiment [17]. Gouy proposed a model for the DL in 1908 that was improved by Chapman and Stern. It is called Gouy-Chapman-Stern model, for which an analytical solution exists. However, this model assumes no reaction and static boundary conditions. Most of the calculations for the DL behavior published produce equivalent capacitance and ion concentration distribution for metal/ionic liquid interface under assumption that no reaction takes place [19]. Other researcher experimentally measured properties of the DL for carbon aerogel/NaF solution like capacitance and resistance, when changing the average pore size, bulk concentration, and solid potential. The results were used to validate the model [20].

In fact, the potential in Gouy-Chapman-Stern model is described using the Poisson–Boltzmann equation, which entropy term is modified by Borukhov, where the contribution of unoccupied space in DL is considered. This consideration allows for a limitation on the maximum ion concentration in DL even if there is a high potential difference between the solid and electrolyte. As a result, calculation accuracy was increased at a high potential [21]. Based on the idea above, Kilic improved the model for static [22] and dynamic behavior [23]. Dynamics are reflected by setting the average concentration and the concentration difference between anion and cation as the two state variables. However, all of these approaches above have assumed no reactions at interface of li-ion cell porous electrode.

The model we propose for DL is based on the Gouy-Chapman-Stern principle and considers reactions at the interface. The static Butler–Volmer equation appeared in the previous electrochemical model [13] [14] is replaced by the one from the DL model. In addition, the equation that describes ion transport in the electrolyte is modified to include the frequency response in the medium range. Moreover, the transference number is no more constant but is a function of cations and anions fluxes. With the improvements incorporated into the electrochemical model, the model covers the complete range of the EIS response that includes the high frequency range. The new electrochemical model including the DL is capable of representing not only the behaviors in the time but also in the frequency domain.

2. Development of a model

Basic unit used for modeling the Li-ion battery is the microcell that has a structure of a sandwich composed of five layers: a negative current collector, anode, separator, cathode, and positive current collector, as shown in Fig. 2. The anode and cathode are composite electrodes that are porous and made of mixed electrolyte and particles. It is assumed that the particles have a spherical shape and are uniformly distributed. The electrolyte adjoining to particles is divided into two areas, bulk area and DL. The bulk area is the one, where the concentration distribution of the anion is equal to that of cation, so the region is electrically neutral. Conversely, the DL located outside the electrode particles between electrodes and the bulk area is not electrically neutral because of the abrupt change of the potential. The DL has a thickness of 1–10 nm. The DL is depicted with cations (red color) and anions (yellow color) (in web version), as shown in Fig. 2. The Stern plane is the closest layer to the particle surface and about 0.2 nm thick, where the anions can approach. It is assumed that the width between the Stern plane and the solid surface is equal to the sum of an anion ion and a solvent molecule size [17].

Transport of each of ions in the DL is affected by their own local chemical potential gradient determined by the electric static potential and the ion concentration gradient. For Li-ion battery, lithium ion is cation, while PF_6^- is the anion resulting from the salt, $LiPF_6$. The lithium ions travel through the DL and participate in

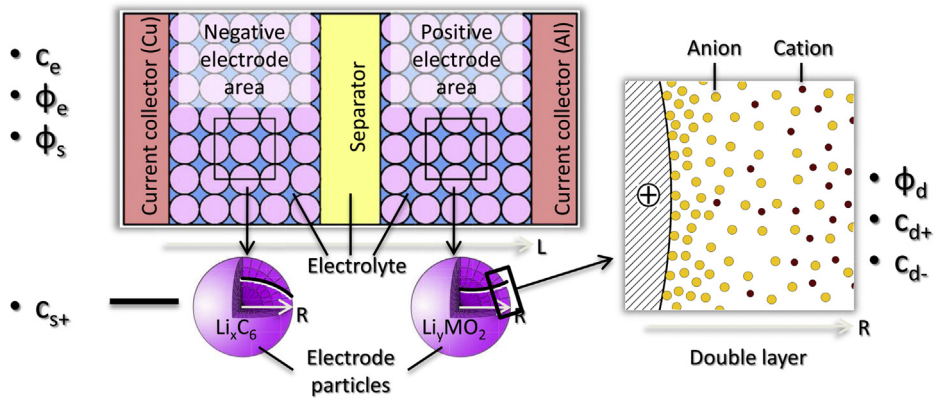

Fig. 2. Set-up for high frequency Li-ion cell modeling.

chemical reactions at the surface of the solid particles while the anions that do not take part in chemical reactions are blocked outside of the Stern plane. Therefore, only cations are participating in the current flow inside Stern layer. The cation ions enter the electrode particles after chemical reaction and continue diffusing until the gradient of the concentration becomes zero. In contrast, the current in bulk and diffuse layer of electrolyte is by both anions and cations. To study mechanism of ion transport, two different coordinates in R and L direction for DL and bulk regions are used. L is the coordinate for the through-the-plane that includes composite anode, separator, and composite cathode, while R is the coordinate for the radial direction that includes electrode particle and DL. The two coordinates are orthogonal to each other. Ions flux in L coordinate is very high compared to that in R coordinate because the ion flux in L direction is the sum of total ion fluxes given in R direction of a particle. However, the potential and concentration gradient in R direction is much higher than that in L direction because of the high potential of the DL. Therefore, it is assumed that the effective mobility of both ions in the DL is smaller than that in the bulk.

2.1. Ion concentration and potential distribution in electrolyte

The bulk region and DL are parts of electrolyte. Potential distribution and ion concentration in electrolyte are derived from the principle of thermodynamics. The Helmholtz free energy is the useful work given by a difference between the internal energy and the entropy term. The energy tends to take the lowest level.

$$A = U - T \cdot S \tag{6}$$

where A is the Helmholtz energy, U is the internal energy, T is temperature and S is the entropy.

Since the electrolyte consists of dielectric solvent, cations and anions, the internal energy can be expressed by the three terms, the energy of static electric field, cations, and anions:

$$U = -\frac{E}{2}|\nabla\phi|^2 + F \cdot c_+ \cdot \phi - F \cdot c_- \cdot \phi \tag{7}$$

where E is the permittivity of dielectric solvent, F is the Faraday's constant, c_+ and c_- are the concentration of cations and anions, respectively, and ϕ is the potential field.

Since the electrolyte has a constant volume, the entropy in the volume can be expressed as a function of the concentration using the lattice gas formulation [21]:

$$S = -R \cdot c_+ \cdot \ln c_+ - R \cdot c_- \cdot \ln c_- - R \cdot \left(\frac{1}{N_A \cdot a^3} - c_+ - c_-\right) \cdot \ln\left(\frac{1}{N_A \cdot a^3} - c_+ - c_-\right) \tag{8}$$

where R is the ideal gas constant and N_A is the Avogadro constant. Anion and cation are assumed to be the same diameter, a.

The last term is the contribution of the free space that is not occupied by either ion. When the ion concentration is as high as the order of the theoretical maximum value $N_A^{-1}\ a^{-3}$, then the free space is low and the term becomes larger.

As a result, the Helmholtz free energy is expressed as a function of the potential and ion concentration. In order to calculate the minimum value of the energy, the Helmholtz energy equation is differentiated with respect to the potential and concentration. The first one yields the Poisson–Boltzmann equation:

$$\frac{\partial A}{\partial \phi} = E \cdot \nabla^2\phi + F \cdot \left(c_+ - c_-\right) = 0 \tag{9}$$

The equation above is not a function of the time.

The second one delivers a relationship for a chemical potential that determines transport of the ion species:

$$\mu_\pm = \frac{\partial A}{\partial c_\pm} = \pm F \cdot \phi + R \cdot T \cdot \left(\ln c_\pm - \ln\left(\frac{1}{N_A \cdot a^3} - c_+ - c_-\right)\right) \tag{10}$$

The equation above is then used to calculate ion flux in the charge conservation equation.

2.2. Ion transport in electrolyte bulk

The current in the bulk can be expressed using ion flux density of cations and anions:

$$i_e = F \cdot (N_{e+} - N_{e-}) \tag{11}$$

where the subscript e denotes the bulk, i is the ionic current density, F is the Faraday constant, N_+ and N_- are the ion flux density of cation and anion, respectively.

Since the charges should be conserved in the bulk region and the bulk is electrically neutral, the cation and anion should have the same concentration distribution. Thus, the charge conservation equation for through-the-plane direction will be:

$$\frac{\partial c_e}{\partial t} = -\frac{\partial N_{e+}}{\partial l} + \frac{j_{E+}}{F}$$
$$\frac{\partial c_e}{\partial t} = -\frac{\partial N_{e-}}{\partial l} + \frac{j_{E-}}{F} \quad (12)$$

where c_e is the concentration of cation and anion, l is the coordinate variable for the through-the-plane direction, N_{e+} and N_{e-} are the ion flux density of cation and anion, respectively, j_+ and j_- are the generation rate of cation and anion from the DL that will be discussed in the following section of DL boundary.

According to the dilute solution transport theory [17], interactions among a solvent and two ion species can be negligible, and the ion transport is only driven by the gradient of corresponding chemical potential that includes the potential and concentration term:

$$N_{e+} = -\frac{\varepsilon_e^{1.5} \cdot b_{e+}}{F} \cdot c_e \cdot \frac{\partial \mu_{e+}}{\partial l}$$
$$N_{e-} = -\frac{\varepsilon_e^{1.5} \cdot b_{e-}}{F} \cdot c_e \cdot \frac{\partial \mu_{e-}}{\partial l} \quad (13)$$

where ε_e is the porosity of electrolyte, 1.5 is Bruggeman's porosity exponent [18], b_{e+} and b_{e-} are the mobility of cation and anion, respectively, μ_{e+} and μ_{e-} are the chemical potential of cation and anion.

Since the ion concentration in the bulk is relatively low compared to the theoretical maximum concentration, the last term in equation (10) is negligible:

$$\mu_{e+} = F \cdot \phi_e + R \cdot T \cdot \ln c_e$$
$$\mu_{e-} = -F \cdot \phi_e + R \cdot T \cdot \ln c_e \quad (14)$$

2.3. Ion transport in double layer (DL)

Ion transport in the DL is very similar to that in the bulk region except the spherical coordinate and some other conditions. Schematic diagram for the DL and bulk is depicted in Fig. 3. For numerical calculations in the DL, the first grid is placed at the surface of electrode particle, the second one at the Stern plane, and finally the last grid is at the boundary between the DL and the bulk. Beyond the boundary, it is assumed that the net charge is zero. For SEI layer at anode, the inner boundary is the same as that of the Stern plane, while the outer boundary is placed on a grid dependent upon the actual thickness, which ranges in several nanometers.

Since no ions are generated in the DL, so the equation for the charge conservation becomes:

$$\frac{\partial c_{d+}}{\partial t} = -\frac{1}{r^2} \cdot \frac{\partial \left(r^2 \cdot N_{d+}\right)}{\partial r}$$
$$\frac{\partial c_{d-}}{\partial t} = -\frac{1}{r^2} \cdot \frac{\partial \left(r^2 \cdot N_{d-}\right)}{\partial r} \quad (15)$$

where r is the variable in the radial coordinate, and the subscript, d, denotes the DL.

Hence, ion flux of cations and anions in the DL can be calculated based on equation (10) for the chemical potentials as follows. Since the anion concentration near the electrode surface is very high, the last term of equation (10) is not negligible compared to that in the bulk. In addition, the Poisson–Boltzmann equation should be used for calculation of the chemical potential given in equation (9) instead of the electrically neutral condition in bulk region.

$$N_{d+} = -\frac{b_{d+}}{F} \cdot c_{d+} \cdot \frac{\partial \mu_{d+}}{\partial r}$$
$$N_{d-} = -\frac{b_{d-}}{F} \cdot c_{d-} \cdot \frac{\partial \mu_{d-}}{\partial r} \quad (16)$$

2.4. Boundary conditions for DL

The DL in the spherical coordinate has two boundaries, the outer boundary with bulk and the inner boundary with electrode particles. At the outer boundary, the coordinate of the DL is different from that of the bulk, but the ion flux at the both sides is the same.

If the specific surface area is defined as the surface area of boundary per unit volume, a_S and a_E, the interface between particle and DL and the interface between the DL and bulk electrolyte can be expressed as below:

$$a_S = \frac{3\varepsilon_S}{R_S}$$
$$a_E = \frac{(R_S + \delta_D)^2}{R_S^2} \cdot a_S \quad (17)$$

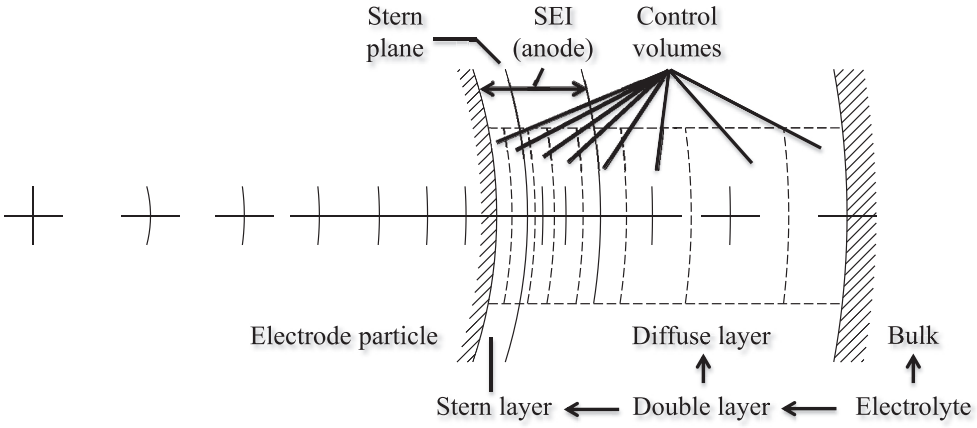

Fig. 3. Meshing of electrode particle and double-layer considering SEI layer.

where ε_S is the volume fraction of electrode, R_S is the average radius of electrode particle, δ_D is the thickness of the DL.

Then, the ion flux at the interface between DL and bulk is as follows:

$$\begin{aligned} j_{E+} &= a_E \cdot F \cdot N_{d+,E} \\ j_{E-} &= a_E \cdot F \cdot N_{d-,E} \end{aligned} \tag{18}$$

When a chemical reaction takes place, corresponding bond energy is needed for enabling the reaction, which is a function of SOC. The energy needed for the reaction of a single ion is called the reaction equilibrium potential, $U_{S,\text{equ}}$, that is the difference between the chemical potentials in the solid and the electrolyte divides Faraday constant. Thus, the chemical potential of electrolyte phase lithium ion at the electrode surface is.

$$\begin{aligned} \mu_{s+} &= F \cdot \phi_s + R \cdot T \cdot \ln c_{s,d} \\ F \cdot U_{S,\text{equ}} &= \mu_{s+} - \mu_{d,s+} \\ \mu_{d,s+} &= F \cdot (\phi_s - U_{S,\text{equ}}) + R \cdot T \cdot \ln c_{s,d} \end{aligned} \tag{19}$$

where the subscript d denotes the DL, $c_{s,d}$ is the lithium ion solid phase concentration at the surface, and ϕ_s is the electric static potential of solid.

According to the charge conservation, the number of electrons participating in reactions is the same as those of ions. As electrons are negative charges, so the current generation by electrons in the solid equation (22) can be calculated from the lithium ion flux at interface between the electrode and the DL.

$$j_{S+} = a_S \cdot F \cdot N_{d+,S} \tag{20}$$

Since the Stern plane is so close to the surface of the solid, no anion can reside within the plane, so that there is no anion flux from the Stern plane to the electrode surface.

$$N_{d-,S} = 0 \tag{21}$$

2.5. Effect of SEI on DL

SEI layer formed at anode is composed of a mixture of organic materials such as $(CH_2OCO_2Li)_2$ and inorganic materials such as Li_2Co_3, LiF, and Li_2O [24]. Most of the organic materials are at outer layer of SEI/electrolyte interface while the majority of the inorganic materials are at inner layer of anode/SEI interface [25]. The two organic and inorganic materials have different properties. According to an isotope experiment [26], the inner SEI layer allows only cation to pass through and has a small diffusion coefficient, while the outer layer allows both cation and anion to pass through. A model for this separated transport mechanism is proposed by S. Shi [27], where the inner layer is described using "interstitial knock-off" mechanism and the outer layer using ordinary porous diffusion. These two layers act like the Stern and diffuse layer proposed in this paper, but the parameters are different. Therefore, the both SEI layers are approximated with the two layers where DL parameters including outer SEI layer thickness, permittivity, ions mobility, and Stern layer thickness are fitted.

2.6. Electrode

The current in electrode is determined by electrons flowing in the thickness direction, which is governed by Ohm's law.

$$\frac{\partial}{\partial l}\left(\sigma^{\text{eff}} \cdot \frac{\partial}{\partial l}\phi_s\right) = j_{S+} \tag{22}$$

where σ^{eff} is the conductivity of electrode, and j_{S+} is the charge generation term that is defined as positive when the current flows from the electrode to DL.

The lithium ion in electrode particles is assumed only to be transported in the radius direction driven by a concentration gradient.

$$\frac{\partial c_s}{\partial t} = \frac{D_s}{r^2}\frac{\partial}{\partial r}\left(r^2 \frac{\partial c_s}{\partial r}\right) \tag{23}$$

where c_s is solid phase lithium ion concentration, r is the radius, and D_s is the diffusion coefficient.

3. Numerical analysis

3.1. Double layer without electric load

When no current flows through the external circuit, the terminal voltage is the same as the open circuit voltage (OCV) that ranges from three to 4 V for Li-ion battery depending upon SOC. The OCV is

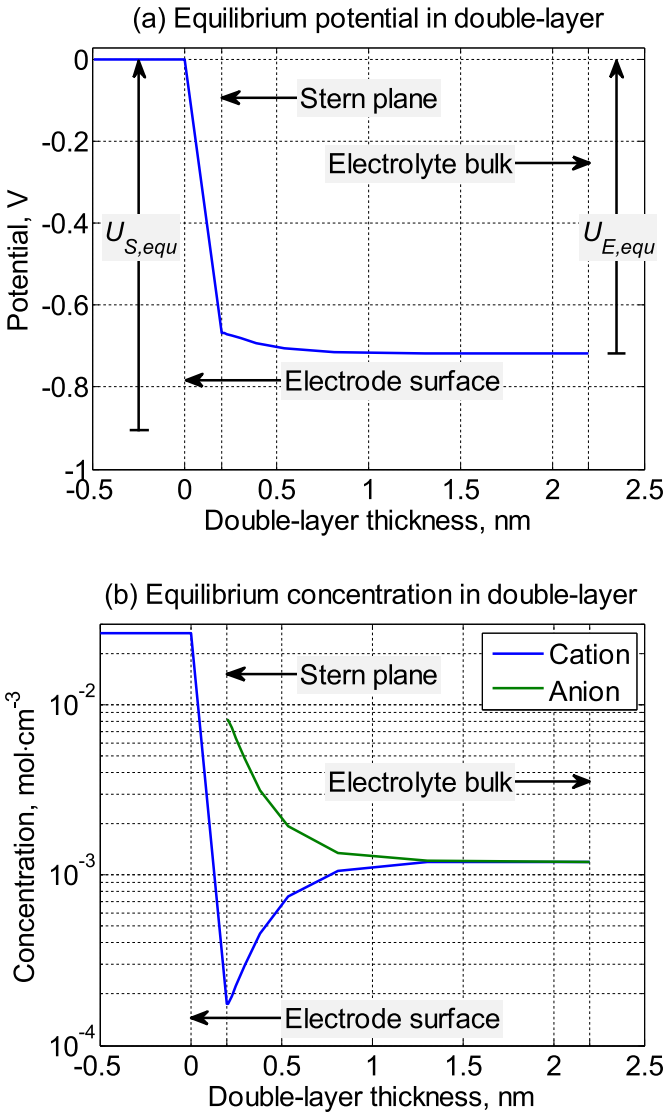

Fig. 4. Equilibrium potential and ion concentration in the DL at anode side.

generally determined by the equilibrium potentials between solids and electrolyte, where the potential at the interface is determined by Butler–Volmer equation and has discontinuity because of the neglected DL. In fact, the potential should be continuous, simply because the first term for the potential in Poisson–Boltzmann goes to infinity when the potential changes with discontinuity. The potential drops dominantly occur at the DL rather than those in electrolyte bulk or electrodes because the total Helmholtz free energy in the DL has the lowest value. At the equilibrium state where no reaction takes place, the chemical potentials of the solid and electrolyte are the same. The reaction equilibrium potential, $U_{s,equ}$, present in the chemical bond attract lithium ions from the electrolyte toward the solid, so that the concentration at the interface becomes low and a concentration gradient is formed across the DL. As a result, the electrostatic potential is changed according to equation (10) as well as the concentration of the anions. Calculated potentials and concentration of ions in the DL is plotted in Fig. 4. The potential gradient outside the Stern plane is lower than the inside because the anions are attracted and the gradient of potential is reduced, in contrast, no anion can reside inside the Stern plane so the highest potential drop occurs from electrode surface to the Stern plane. The net balance of charges reaches its maximum at the Stern plane and becomes zero at the bulk as well as the potential gradient.

The reaction equilibrium potential, $U_{S,equ}$, used for calculation is 0.91 V, as in Fig. 4(a). The difference between the solid and bulk potential, called the double-layer equilibrium potential, $U_{E,equ}$, is 0.72 V, which is a function of variables like the solid phase lithium ion concentration, equilibrium potential, bulk concentration, and electrolyte permittivity. The first two variables are a function of SOC and different at anode and cathode. Particularly, the double-layer equilibrium potential is used as the equilibrium potential in Butler–Volmer equation. The difference between the reaction and the double-layer equilibrium potentials at anode and cathode are plotted in Fig. 5.

The results shows that the equilibrium potential difference at anode side tends to follow the increase of SOC, while at cathode side inversely proportional to SOC.

In order to analyze the effects of the SOC on the concentration in the DL, ion distributions in the DL at the equilibrium state are plotted in Fig. 6 as a function of SOC. The anion (PF_6^-) has higher concentration than the cation (Li^+) because of the positive equilibrium potential. In addition, the lithium ion concentration

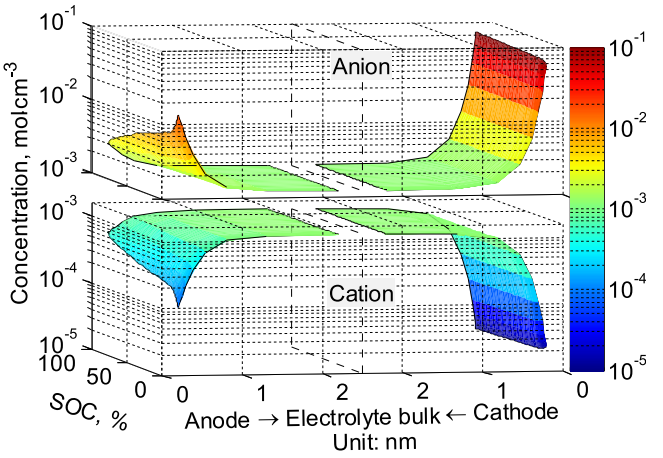

Fig. 6. Equilibrium ion distributions in DL as a function of SOC.

becomes lower near the cathode surface, so a high chemical potential gradient is needed to maintain the same rate of ion flux, which results in a high resistance compared to that in anode. Moreover, the ion concentration at the cathode is not affected by SOC, while the concentration at anode surface is heavily influenced because the equilibrium potential change at anode is more than 60% while that at cathode is only 20% when operated at different SOC. The ion concentration at the anode between 0% SOC and 100% SOC is six and thirty times higher than that at the cathode surface, which might be one of causes for the lithium plating that is particularly formed at anode side when operated at high SOC range.

3.2. Double layer with constant DC current load

Calculated resistances of the DL on the anode (blue line) and cathode (green line) as well as the total resistance as a function of current densities are plotted in Fig. 7. The results of the calculation show that the film resistance on the anode DL (blue line) decreases when discharged and the current density increases, while that of cathode DL (green line) (in web version) increases when discharged. However, the total resistance is not symmetric to the direction and magnitude of the current density. The total resistance

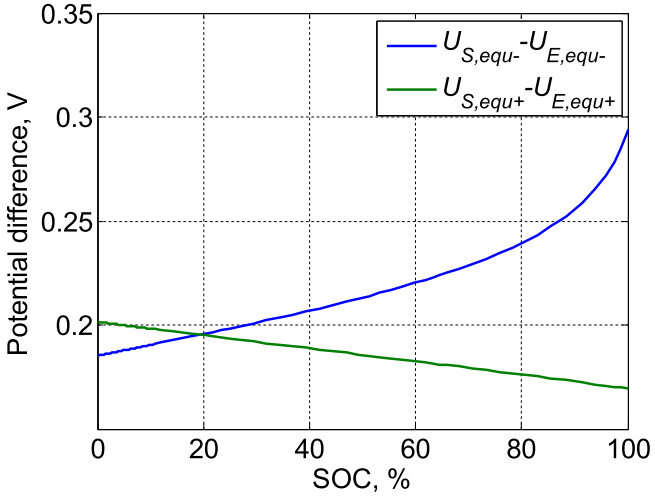

Fig. 5. Difference between the two equilibrium potentials as a function of SOC.

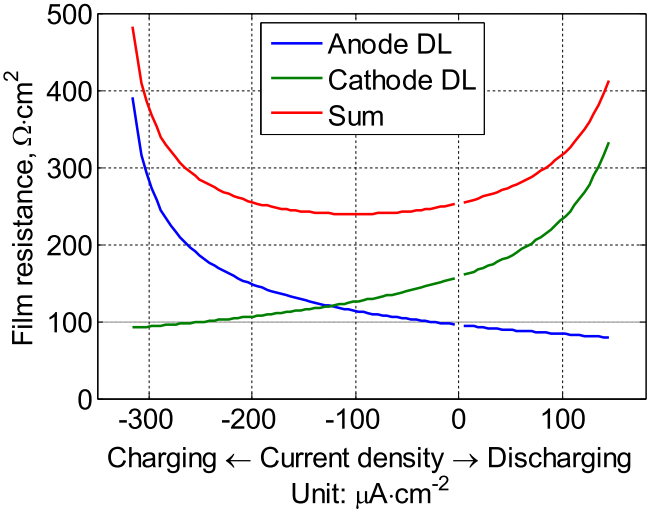

Fig. 7. Film resistance of DL as a function of constant current density.

varies from two or three times larger than that at the lowest value, as plotted in red color.

The resistance values shown above are different from that calculated using Butler–Volmer equation. The resistance by the Butler–Volmer equation is constant at small currents and increases when charging and discharging the cell with high currents. In addition, the minimum value was at the zero current. The analysis, however, shows that the minimum value of the resistance considering the DL is not at zero current. The resistance in the anode DL was at the lowest value when discharged with high currents and in the cathode when charged with high currents. These asymmetric resistance values are caused by the direction of the current flowing from solid to electrolyte and the resulting positive equilibrium potentials. The sum of the DL resistance for two electrodes has reached its minimum value when charging the battery with 100 μA cm^{-2}.

In fact, this current density depends on other variables like SOC, particle sizes used for two electrodes, and volume of two electrodes. The resistance as a function of current density and the SOC is plotted in Fig. 8 under assumption that the particle sizes and volumes of two electrodes are the same. The DL resistance is independent upon SOC when discharging because the resistance is dominantly determined by the cathode DL resistance. In addition, the DL resistance at charging has been always less than that at discharging when the absolute values of currents are the same. The DL resistance at low SOC and charging is much larger than that at high SOC.

3.3. Double layer with AC current load

Analysis of the DL at equilibrium states shows that cation concentration near the surface of electrodes can be one several thousandth of anion concentration or even smaller dependent upon equilibrium potential and the permittivity of dielectric solvent. On the other hand, the cations move very fast in DL at a given ion flux that is determined by the current density, which implies that cations in a certain control volume will depart within a very short time when charging or discharging currents are not zero. Therefore, cations given in the previous time step completely departed the control volume that will be filled up with the new cations in the current time step. The lithium ion conservation equation (15) is replaced by a static equation obtained from the charge conservation, which improves the numerical accuracy, even ignored dynamics for the cations:

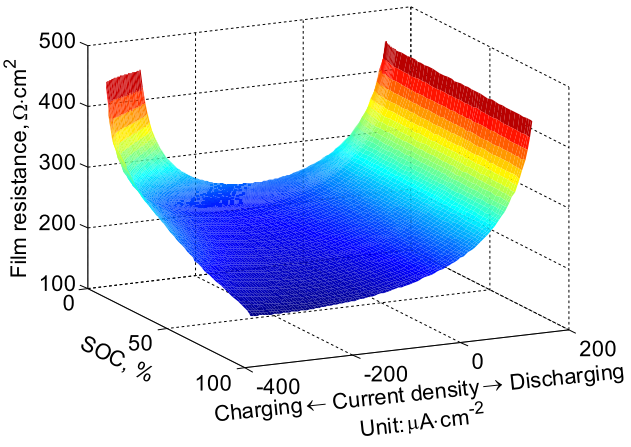

Fig. 8. DL film resistance as function of SOC and current.

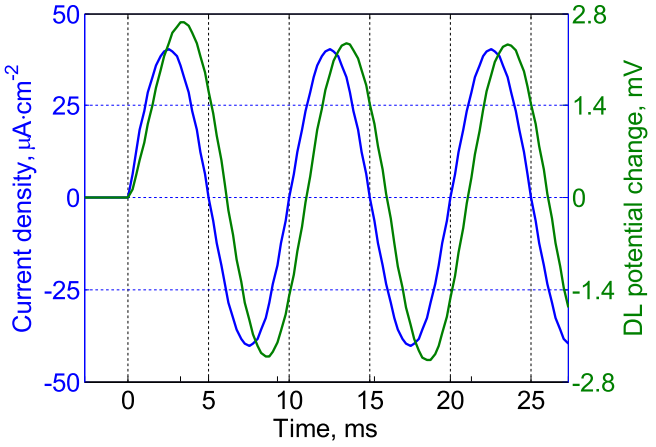

Fig. 9. Potential response of DL on anode side.

$$\frac{\partial}{\partial r}\left(r^2\cdot N_{d+}-r^2\cdot N_{d-}\right)=0$$
$$\frac{\partial c_{d-}}{\partial t}=-\frac{1}{r^2}\cdot\frac{\partial\left(r^2\cdot N_{d-}\right)}{\partial r} \quad (24)$$

The response of an AC current load with a frequency of 100 Hz using equation (24) on the potential of the anode DL is plotted in Fig. 9, where the effects of the cations have not considered. The steady state of the potential has been reached after half of the first period.

Based on the relationship between the AC currents and potentials, the Nyquist plot for impedances of the anode DL is drawn in Fig. 10. When the frequency of the current varies from 1 Hz to 10 kHz, the value of the impedance varies too and becomes a shape of a semicircle.

3.4. Effects of SEI on DL AC impedance

As described, SEI layer causes increase of DL permittivity and decrease of DL ions mobility. The resulting effects are plotted in Fig. 11. When the ion mobility gets smaller or permittivity does larger, the semi-circle gets bigger. Ions need more activation energy to overcome atomic force present in the SEI material and as a result the ion mobility in SEI becomes much smaller than that in electrolyte [27]. Consequently, the significantly high DL impedance is

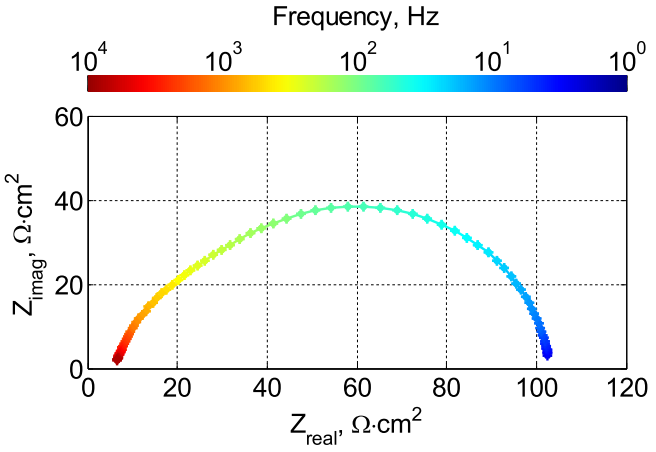

Fig. 10. Nyquist plot of anode DL impedance.

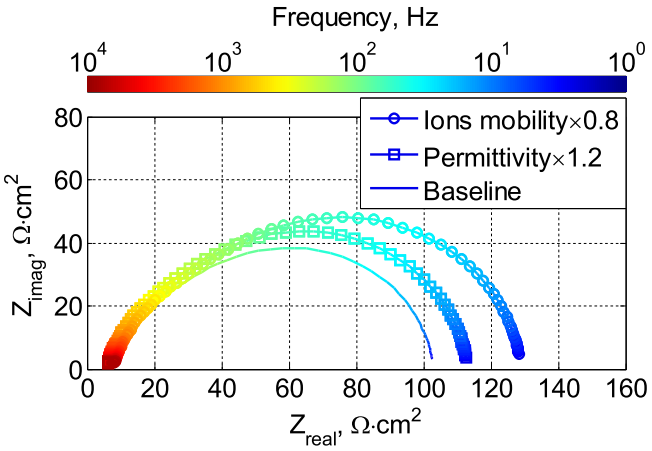

Fig. 11. Effects of SEI on DL AC impedance.

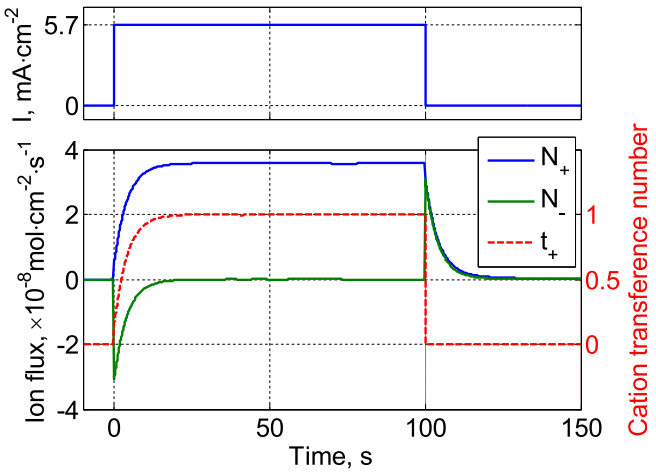

Fig. 13. Average ion flux and transference number in bulk when discharging.

induced by the SEI. Detailed parameters dependency on SEI formation and degradation will be investigated in the future work.

3.5. Bulk

Bulk is the region where the same number of cations and anions are present at every control volume and becomes overall electrically neutral. Even if both ions have the same concentration distribution in the bulk, they are not paired but move separately. Since the cations are more generated or absorbed than anions in the DL, more cations are crossing the boundary between the DL and the bulk. Corresponding numbers of anions leave or enter the control volume of bulk to keep the neutrality.

Both distributions of ion concentration and ion fluxes in the bulk at 0.1, 4.7 and 62.7sec during discharging and at 102.3sec during resting are calculated and plotted in Fig. 12, where the direction of ion movements are marked with half arrow, which color and length indicate the magnitude of the flux. The ion concentration (a) at 0.1sec shortly after discharging is uniformly distributed. Both ions are moving in opposite directions, where anions move toward anode, while cations do toward cathode, which is caused by the electrostatic potential gradient. The magnitude of anions flux is larger than that of cation flux at the beginning of discharge simply because of the high ion mobility of the anion. As the anions do not participate in any reactions taking place in both electrodes, the transported anions are accumulated more in anode and less in cathode. Therefore, a concentration gradient is formed. This gradient produces a diffusion force exerting on the ions, so cations are accelerated and the flux gets increased. Conversely, anions are decelerated and the flux becomes decreased, as shown in (b).

At 62.7sec, the concentration distribution reaches a steady state, where the net flux of anion becomes zero, but the flux of cation becomes the highest, as shown in (c), which implies that the ionic current in the bulk is only determined by cation flux. At 102.3sec during resting, where no load current is applied, a concentration gradient is still present and drives ions until evenly distributed. Thus, both cations and anions move in the same direction, which fluxes have the same magnitude. As a result, no net current flows in the bulk, as shown in (d). In addition, the ion flux get high in separator region but low near current collectors since the ions are generated and accumulated in the composite electrodes.

The transference number is generally defined as a contribution of ion species to a total current flow. Transference number for cations and the associated ion fluxes during discharging and resting as a function of time are plotted in Fig. 13, where a step discharge current (the first plot with Blue line) is applied. The transference number becomes no more constant. At the instant when the discharging current is applied, the transference number increases to 1/7 instantly because the chosen mobility of anions is six times higher

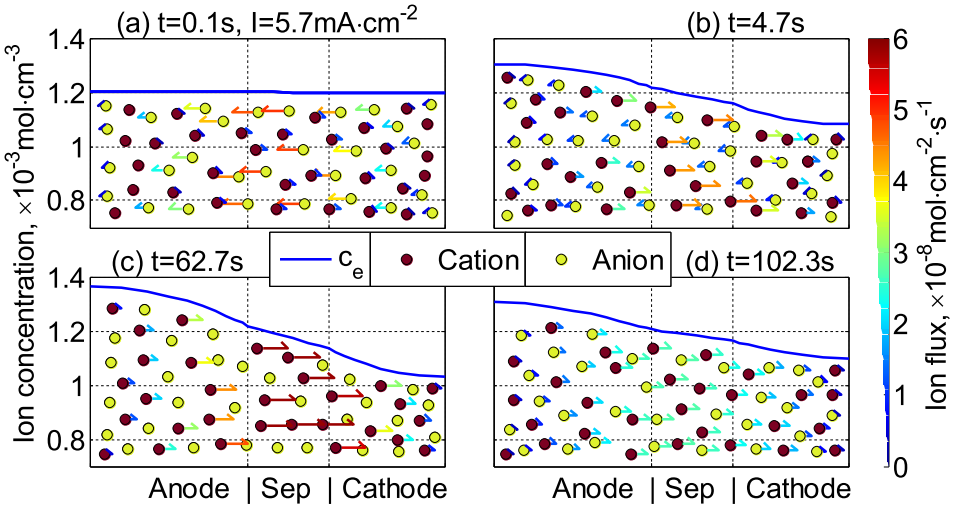

Fig. 12. Ion concentration and fluxes in the bulk.

than that of cations. Accordingly, the anion and the cation flux jumps to one seventh and six seventh of the total flux, respectively. Due to the participation of the ions in current flow and resulting effects of the concentration gradients as described above, the anion flux gets decreased as the time passes by, while the cation flux gets increased until the concentration gradient reaches its maximum.

When the current goes to zero, there are still ion fluxes caused by the concentration gradient present in the bulk until having the ions evenly distributed. At the instant when the abrupt current change occurs, both fluxes have the same magnitude and decay according to the decreasing concentration gradient with a time constant determined by ions mobility. At the same time, transference number becomes infinite.

4. Integration of the model for double layer and validation

4.1. Summary of integrated model

The sub-models for the DL and bulk are integrated into the model developed for a microcell described in previous chapters. The model is summarized in table below.

- Double layer potential
  - Equation

$$E\cdot\frac{\partial^2\phi_d}{\partial r^2}+F\left(c_{d+}-c_{d-}\right)=0 \tag{25}$$

  - Boundary condition

$$\phi_d|_{r=R_S}=\phi_s,\quad \phi_d|_{r=R_S+\delta_D}=\phi_e \tag{26}$$

- Double layer ion transport
  - Equation

$$\begin{gathered}\frac{\partial c_{d-}}{\partial t}=\frac{b_{d-}}{F\cdot r^2}\cdot\frac{\partial}{\partial r}\left(r^2\cdot c_{d-}\cdot\frac{\partial\mu_{d-}}{\partial r}\right)\\ -\frac{3\cdot\varepsilon_S\cdot r^2}{R_S^3}\cdot\left(b_{d+}\cdot c_{d+}\cdot\frac{\partial\mu_{d+}}{\partial r}-b_{d-}\cdot c_{d-}\cdot\frac{\partial\mu_{d-}}{\partial r}\right)=j_{S+}\\ \text{where}\quad \mu_{d+}=F\cdot\phi_d+R\cdot T\cdot\left(\ln c_{d+}-\ln\left(\frac{1}{N_A\cdot a^3}-c_{d+}-c_{d-}\right)\right)\\ \mu_{d-}=-F\cdot\phi_d+R\cdot T\cdot\left(\ln c_{d-}-\ln\left(\frac{1}{N_A\cdot a^3}-c_{d+}-c_{d-}\right)\right)\\ j_+=-\frac{3\varepsilon_S\cdot b_{d+}}{R_S^3}\cdot r^2\cdot c_{d+}\cdot\frac{\partial\mu_{d+}}{\partial r},\quad j_{S+}=j_+|_{r=R_S}\\ j_-=-\frac{3\varepsilon_S\cdot b_{d-}}{R_S^3}\cdot r^2\cdot c_{d-}\cdot\frac{\partial\mu_{d-}}{\partial r}\end{gathered} \tag{27}$$

  - Boundary condition

$$\begin{gathered}c_{d-}|_{r=R_S+\delta_D}=c_e,\quad \frac{1}{r}\cdot\left.\frac{\partial\mu_{d-}}{\partial r}\right|_{r=R_{ST}}=0\\ c_{d+}|_{r=R_S+\delta_D}=c_e,\quad \mu_{d+}|_{r=R_S}=F\left(\phi_s-U_{s,equ}\right)+R\cdot T\cdot\ln c_{s,d}\end{gathered} \tag{28}$$

- Electrolyte ion transport
  - Equation

$$\begin{gathered}\frac{\partial(\varepsilon_e\cdot c_e)}{\partial t}=\varepsilon_e^{1.5}\cdot b_{e+}\cdot\frac{\partial}{\partial l}\left(c_e\cdot\frac{\partial}{\partial l}\left(\phi_e+\frac{R\cdot T}{F}\cdot\ln c_e\right)\right)+\frac{j_{E+}}{F}\\ \frac{\partial(\varepsilon_e\cdot c_e)}{\partial t}=\varepsilon_e^{1.5}\cdot b_{e-}\cdot\frac{\partial}{\partial l}\left(c_e\cdot\frac{\partial}{\partial l}\left(-\phi_e+\frac{R\cdot T}{F}\cdot\ln c_e\right)\right)+\frac{j_{E-}}{F}\\ \text{where}\quad j_{E+}=j_+|_{r=R_S+\delta_D}\\ j_{E-}=j_-|_{r=R_S+\delta_D}\end{gathered} \tag{29}$$

(*continued*)

  - Boundary condition

$$\begin{gathered}\left.\frac{\partial c_e}{\partial l}\right|_{l=0}=\left.\frac{\partial c_e}{\partial l}\right|_{l=L}=0\\ \phi_e|_{l=0}=0,\quad \left.\frac{\partial\phi_e}{\partial l}\right|_{l=L}=0\end{gathered} \tag{30}$$

- Solid phase ion transport
  - Equation

$$\frac{\partial c_s}{\partial t}=\frac{D_s}{r^2}\frac{\partial}{\partial r}\left(r^2\frac{\partial c_s}{\partial r}\right) \tag{31}$$

  - Boundary condition

$$\frac{1}{r}\cdot\left.\frac{\partial c_s}{\partial r}\right|_{r=0}=0,\quad D_S\cdot\left.\frac{\partial c_s}{\partial r}\right|_{r=R_s}=-\frac{j_{S+}}{a_S\cdot F} \tag{32}$$

- Solid conductive
  - Equation

$$\frac{\partial}{\partial l}\left(\sigma^{\text{eff}}\cdot\frac{\partial}{\partial l}\phi_s\right)=j_{S+} \tag{33}$$

  - Boundary condition

$$\begin{gathered}\sigma_-^{eff}\cdot\left.\frac{\partial\phi_s}{\partial l}\right|_{l=0}=\sigma_+^{eff}\cdot\left.\frac{\partial\phi_s}{\partial l}\right|_{l=L}=-\frac{I}{A}\\ \left.\frac{\partial\phi_s}{\partial l}\right|_{l=\delta_-}=\left.\frac{\partial\phi_s}{\partial l}\right|_{l=L-\delta_+}=0\end{gathered} \tag{34}$$

4.2. Impedance measurements

The battery used for the experiments is a pouch type power cell with dimension of active materials about 20 cm × 15 cm × 0.5 cm and made of $LiMn_2O_4$ and carbon. Its capacity is 15.7 Ah and the operating voltage is from 2.5 V to 4.15 V. The test station was constructed using a DC power supply and an electronic load. LabVIEW embedded in a PC was used to control power supply, e-load and heat pumps, as depicted in Fig. 14. A high resolution current transformer and two thermocouples were employed to accurately measure the current and the surface temperatures. Two thermocouples were located on the both sides of the battery center.

Before measurements of the impedances, SOC of the battery is firstly set to be 50% and then AC sinusoidal waveforms generated by LabVIEW codes are amplified and applied to the terminal, which amplitude is 3 A and frequency varies from 1 mHz to 1 kHz. In order to investigate effects of temperature on impedances, the two heat pumps are extra used to control the surface temperature of the battery at a set value. The range of the controlled temperature is from 0 °C to 40 °C. Under a set temperature, terminal AC current and voltage at a given frequency are measured for several periods and processed using Fast Fourier Transform (FFT) to obtain their amplitude and phase. Then, the impedance of the signals at the frequency is calculated.

The experiment results are shown in Fig. 15. Impedance is very sensitive to the temperatures. The diameter of the semi-circle at 5 °C is 14 times larger than that at 37 °C, which correspond to 3.6 mΩ and 0.25 mΩ respectively, due to lower mobility of ions in both electrolyte and electrode. However, the impedance becomes resistive and independent upon temperature when the frequency increases because of the major contribution of the resistance in solid phase.

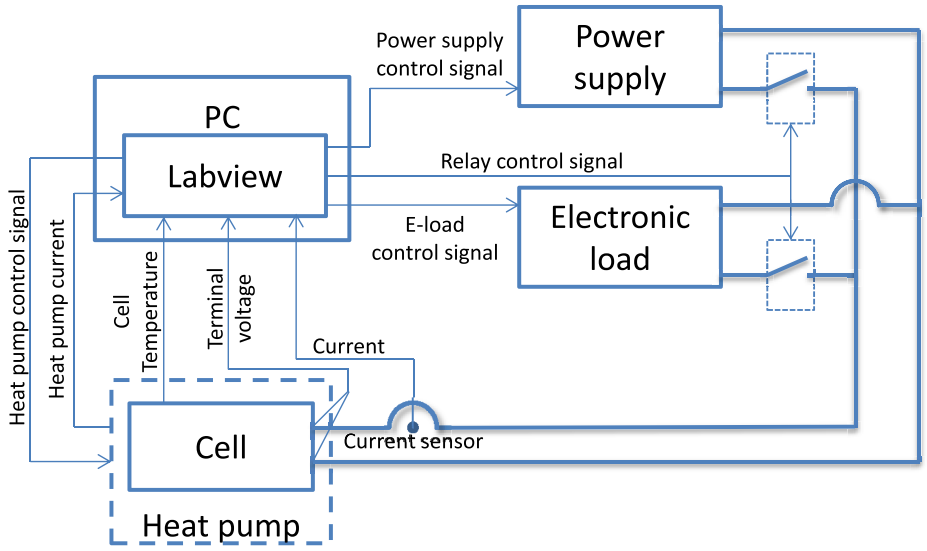

Fig. 14. Schematic diagram of test station.

4.3. Extraction of four parameters

The four parameters needed for the electrochemical model are the mobility in bulk (b_B) and DL (b_D), permittivity (E), and diffusion coefficient in solid (D_s). The parameters are extracted from experiment data using nonlinear least square curve fitting method for the temperature range from 9 °C to 37 °C. Each of the extracted parameters has shown an exponential function with respect to temperature that is the same as Arrhenius equation. The experimental data and the fitted line are plotted in Fig. 16, where the stars and solid lines represent parameters extracted at each temperature and the fitted line in different temperatures compared to that in 25 °C. The reference parameters in 25 °C are listed in appended table. The real and imaginary parts of the impedance model are calculated using the fitted parameters and compared with experimental data, as shown in Fig. 17(a).

The imaginary part of the impedance has shown the highest value when the frequency is zero (DC) and decreases until about 2 Hz. Thereafter, the part increases again until around 20 Hz, and decreases to a minimum when the frequency continuously increases. A sensitivity analysis of the parameters has revealed that the effective radius of electrode particles, which is actually independent upon temperature, affects the frequency where the second peak of the imaginary part occurs. Conversely, the real part of the impedance tends to decrease when the frequency increases and can be categorized into three frequency ranges: 1) high frequency range from 10 to 1000 Hz, where the ions mobility in DL and permittivity play the major role, 2) medium frequency range from 0.05 to 10 Hz, where ions mobility in bulk is responsible for, and 3) low frequency range less than 0.05 Hz, where ion diffusion coefficient in solid is responsible for. The associated Nyquist plots for impedance are shown in Fig. 17(b).

The model is capable of predicting the responses in the high frequency range, but has discrepancies in the low frequency impedance. In fact, the Li-ion diffusion in solid phase determines the low frequency response. More specifically, the slopes of both real and imaginary parts of impedance at low frequency range are affected by only one factor, D_S/R_S^2, where D_S is the diffusion coefficient in solid, and R_S is the average radius of electrode particles. Comparison shows a trend that the calculated impedance for real and imaginary part is larger and smaller than that measured. Since change of D_S/R_S^2 has led to a shift of both parts simultaneously, appropriate parameters for the experiments cannot be found. Thus, we have attempted with three different approaches to find out reasons, reformulation of the diffusion mechanism based on chemical potential gradient instead of concentration gradient,

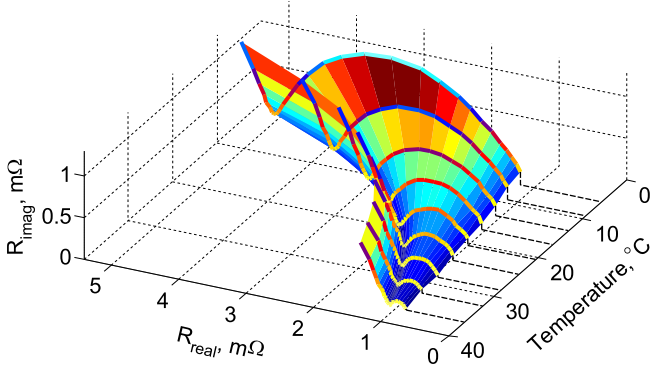

Fig. 15. Measured impedance as function of temperature.

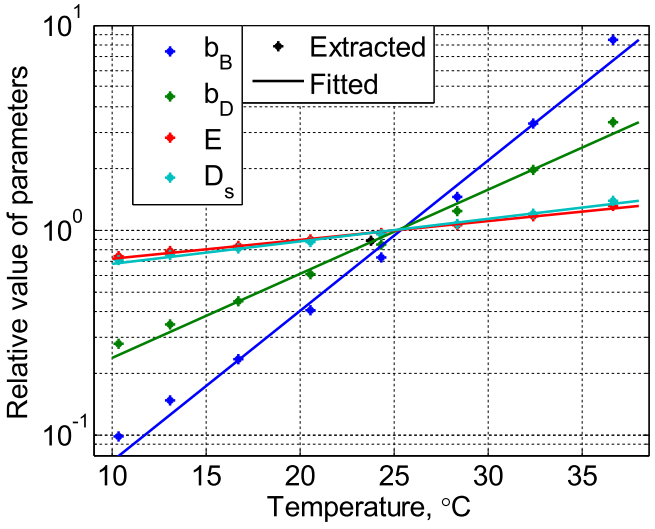

Fig. 16. Extracted parameters and fitted line as function of temperature.

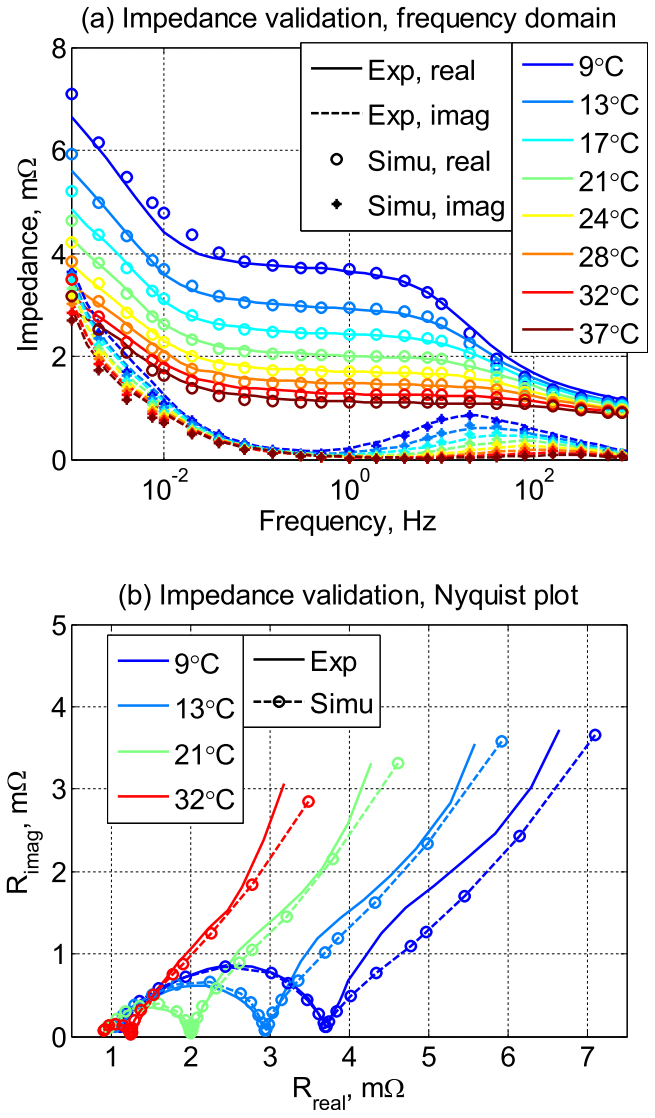

Fig. 17. Validation of impedance model.

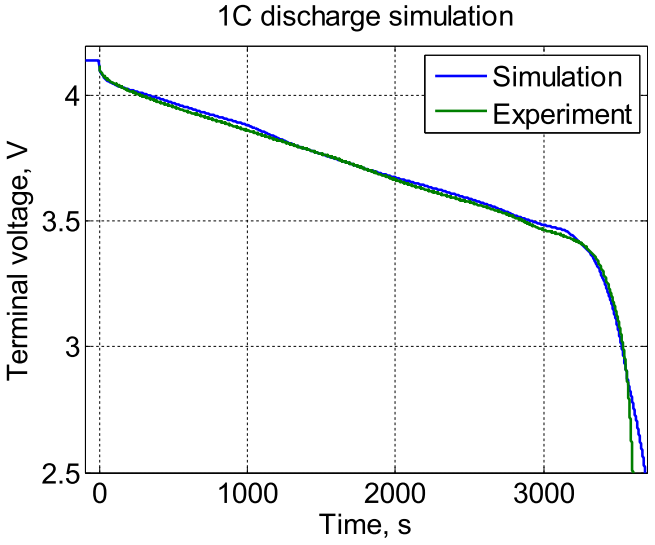

Fig. 18. Comparison of discharging behaviors at 1C rate.

effects of two dimensional geometry of the pouch cells, and finally non-uniform particle sizes in porous electrodes. It turns out that the non-uniform particle radius is only the one that is affecting the differences of the two slopes. Further analysis on low frequency model will be published in the next paper.

However, the response in time domain during 1C discharge, as shown in Fig. 18, shows a fairly good match between the simulation and experiment results in spite of the discrepancy in low frequency impedances.

5. Conclusion

Measurement of impedances of battery is one of well-known methods to experimentally characterize properties of electrochemical devices including Li-ion batteries. The impedance responses are generally fitted to an impedance model that consists of linear and nonlinear electric circuit components. However, it is very hard to find comprehensive correlation between the impedance model parameters and physical phenomena taking place inside of the battery cell. On the other hand, the electrochemical model being widely used for investigation of physical phenomena cannot provide AC response, particularly in the high frequency range resulting from the DL. Therefore, sub-models for the DL and bulk is newly developed and integrated into the electrochemical model for a pouch type Li-polymer battery. The integrated model is validated against experiments in time and frequency domain. The developed model is capable of representing the responses at charging and discharging not only in time domain, but also in the frequency domain. The simulation results show several interesting findings as follows:

- The reaction equilibrium potential that represents energy of chemical bonds is not the same as the DL equilibrium potential used in the Butler–Volmer equation. The difference depends upon the equilibrium potential, SOC, and load condition.
- The cation concentration near to the electrode surface is much lower than that in the bulk, while the anion concentration is higher than that in bulk.
- The cations concentration near to the electrode surface on anode side at 0% and 100% SOC is six and thirty times higher than that at the cathode surface, which might be one of the causes that produce the lithium plating, particularly on the anode side when the SOC is high.
- Resistance of DL at discharging is independent upon SOC because the resistance of the DL on the cathode side is dominant. The DL resistance during the charging is always smaller than that during discharging if the magnitude of currents is the same.
- The transference number varies as the time passes by. The number gradually increases and finally becomes 100% within 1 min during charging or discharging, even though the electrolyte is electrically neutral.
- DL is responsible for the high frequency response that forms the low semi-circle of Nyquist plot that can be observed from EIS measurement, while the bulk and diffusion in the electrode determine the medium and the low frequency response respectively, that forms the linear increasing part of the Nyquist plot.
- Impedances of lithium ion battery is sensitive to the temperature, which is caused by dependency of ions mobility and permittivity on temperature. The ions mobilities are exponential functions with respect to temperature, which agree with the Arrhenius equation.

Appendix. Parameters

	Parameter	Negative electrode	Separator	Positive electrode	unit	Ref.
Design specifications (geometry and volume fractions)	Thickness, δ	$50*10^{-4}$	$25.4*10^{-4}$	$36.4*10^{-4}$	cm	[14]
	Particle radius, R_s	$6.22*10^{-4}$		$6.22*10^{-4}$	cm	a
	Active material volume fraction, ε_s	0.58		0.5		[28]
	Polymer phase volume fraction, ε_p	0.048	0.5	0.11		[28]
	Conductive filler volume fraction, ε_f	0.04		0.06		[28]
	Porosity, ε_e	0.332	0.5	0.33		[28]
	Cation radius, a_+	$1*10^{-8}$		$1*10^{-8}$	cm	b
	Anion radius, a_-	$2*10^{-8}$		$2*10^{-8}$	cm	b
Solid and electrolyte phase Li^+ concentration	Maximum solid phase concentration, $c_{s,max}$	$50.6*10^{-3}$		$134.4*10^{-3}$	mol cm^{-3}	c
	Stoichiometry at 0% SOC: $x_{0\%}$, $y_{0\%}$	0.126		0.936		[14]
	Stoichiometry at 100% SOC: $x_{100\%}$, $y_{100\%}$	0.676		0.442		[14]
	Average electrolyte concentration, c_e	$1.2*10^{-3}$	$1.2*10^{-3}$	$1.2*10^{-3}$	mol cm^{-3}	[28]
Kinetic and transport properties @25 °C & temperature dependency	Solid phase Li diffusion coefficient, D_{s25} $D_s = D_{s25}\cdot\exp(0.025\cdot\Delta T)$	$4.8*10^{-11}$		$9.7*10^{-11}$	$cm^2\ s^{-1}$	d
	Solid phase conductivity, σ	1		0.1	S cm^{-1}	[28]
	Cation mobility in bulk, b_{B25+}	$8.4*10^{-4}$	$8.4*10^{-4}$	$8.4*10^{-4}$	$cm^2\ V^{-1}\ s^{-1}$	e
	Anion mobility in bulk, b_{B25-} $b_{B\pm} = b_{B25\pm}\cdot\exp(0.167\cdot\Delta T)$	$5.0*10^{-3}$	$5.0*10^{-3}$	$5.0*10^{-3}$	$cm^2\ V^{-1}\ s^{-1}$	e
	Cation mobility in DL, b_{D25+}	$1.0*10^{-10}$		$1.0*10^{-10}$	$cm^2\ V^{-1}\ s^{-1}$	a
	Anion mobility in DL, b_{D25-} $b_{D\pm} = b_{D25\pm}\cdot\exp(0.094\cdot\Delta T)$	$6.1*10^{-10}$		$6.1*10^{-10}$	$cm^2\ V^{-1}\ s^{-1}$	a
	Electrolyte permittivity, E_{25} $E = E_{25}\cdot\exp(0.021\cdot\Delta T)$	$1.9*10^{-12}$		$1.9*10^{-12}$	F cm^{-1}	a
	Bruggeman's porosity exponent, p	1.5	1.5	1.5		[18]

a. Fitted from high frequency impedance.
b. Assumed.
c. Calculated from capacity, stoichiometry numbers, and battery geometry.
d. Fitted from low frequency impedance.
e. Fitted from medium frequency impedance.

References

[1] F. Laman, M. Matsen, J. Stiles, J. Electrochem. Soc. 133 (1986) 2441–2446.
[2] N. Munichandraiah, L. Scanlon, R. Marsh, J. Power Sources 72 (1998) 203–210.
[3] G. Ning, B. Haran, B. Popov, J. Power Sources 117 (2003) 160–196.
[4] R. Ramasamy, R. White, B. Popov, J. Power Sources 141 (2005) 298–306.
[5] J. Li, E. Murphy, J. Winnick, P. Kohl, J. Power Sources 102 (2001) 294–301.
[6] C. Chen, J. Liu, K. Amine, J. Power Sources 96 (2001) 321–328.
[7] R. Bouchet, S. Lascaud, M. Rosso, J. Electrochem Soc. 150 (2003) A1385–A1389.
[8] S. Zhang, K. Xu, T. Jow, J. Electrochim. Acta 51 (2006) 1636–1640.
[9] S. Narayanan, D. Shen, S. Surampudi, A. Attia, G. Halpert, J. Electrochem. Soc. 140 (1993) 1854–1861.
[10] J. Lee, O. Nam, B. Cho, J. Power Sources 174 (2007) 9–15.
[11] J. Xu, C. Mi, B. Cao, J. Cao, J. Power Sources 233 (2013) 277–284.
[12] M. Doyle, T. Fuller, J. Newman, J. Electrochem. Soc. 140 (1993) 1526–1533.
[13] M. Xiao, S. Choe, J. Power Sources 218 (2012) 357–367.
[14] M. Xiao, S. Choe, J. Power Sources 241 (2013) 46–55.
[15] I. Ong, J. Newman, J. Electrochem. Soc. 146 (1999) 4360–4365.
[16] M. Doyle, J. Meyers, J. Newman, J. Electrochem. Soc. 147 (2000) 99–110.
[17] D. Grahame, J. Chem. Rev. 41 (1947) 441–501.
[18] T. Fuller, M. Doyle, J. Newman, J. Electrochem. Soc. 141 (1994) 1–10.
[19] K. Oldham, J. Electroanal. Chem. 613 (2008) 131–138.
[20] K. Yang, T. Ying, S. Yiacoumi, C. Tsouris, E. Vittoratos, J. Langmuir 17 (2001) 1961–1969.
[21] I. Borukhov, D. Andelman, H. Orland, J. Electrochim. Acta 46 (2000) 221–229.
[22] M. Kilic, M. Bazant, J. Phys. Rev. E 75 (2007) 021502, http://dx.doi.org/10.1103/PhysRevE.75.021502.
[23] M. Kilic, M. Bazant, J. Phys. Rev. E 75 (2007) 021503, http://dx.doi.org/10.1103/PhysRevE.75.021503.
[24] D. Aurbach, J. Power Sources 89 (2000) 206–281.
[25] K. Kanamura, H. Tamura, S. Shiraishi, Z. Takehara, Electrochim. Acta. 40 (1995) 913.
[26] P. Lu, S. Harris, J. Electrochem. Comm. 13 (2011) 1035–1037.
[27] S. Shi, et al., J. Am. Chem. Soc. 134 (2012) 15476–15487.
[28] M. Doyle, Y. Fuentes, J. Electrochem. Soc. 150 (2003) A706–A713.